clean technologies

MDPI

Article

Sustainable Synthesis of FITC Chitosan-Capped Gold Nanoparticles for Biomedical Applications

Valeria De Matteis [1,*], Loris Rizzello [2,3,4], Mariafrancesca Cascione [1], Paolo Pellegrino [1], Jagpreet Singh [5,6,*], Daniela Manno [1] and Rosaria Rinaldi [1]

1 Department of Mathematics and Physics "Ennio De Giorgi", University of Salento, Via Arnesano, 73100 Lecce, Italy
2 Department of Pharmaceutical Sciences (DISFARM), University of Milan, Via G. Balzaretti 9, 20133 Milan, Italy
3 National Institute of Molecular Genetics (INGM), Via F. Sforza 35, 20122 Milan, Italy
4 Institute for Bioengineering of Catalonia (IBEC), The Barcelona Institute of Science and Technology, Baldiri Reixac 10-12, 08028 Barcelona, Spain
5 Department of Chemical Engineering, Chandigarh University, Mohali 140413, India
6 University Centre for Research and Development, Chandigarh University, Mohali 140413, India
* Correspondence: valeria.dematteis@unisalento.it (V.D.M.); jagpreetnano@gmail.com or jagpreet.e12147@cumail.in (J.S.)

Abstract: The quest for novel nanoscale materials for different applications necessitates that they are easy to obtain and have excellent physical properties and low toxicity. Moreover, considering the ongoing environmental impact of noxious chemical waste products, it is important to adopt eco-friendly approaches for nanoparticle synthesis. In this work, a natural polymer (medium molecular weight chitosan) derived from chitin was employed as a reducing agent to obtain gold nanoparticles (AuNPs) with a chitosan shell (AuNPs@CS) by a microwave oven. The chitosan is economically viable and cost-competitive in the market showing also nontoxic behavior in the environment and living organisms. The synthesized AuNPs@CS-FITC NPs were fully characterized by spectroscopic and microscopic characterization techniques. The size distribution of NPs was about 15 nm, which is a suitable dimension to use in biomedical applications due to their high tissue penetration, great circulation in blood, and optimal clearance as well as low toxicity. The prepared polymer-capped NPs were further functionalized with a fluorescent molecule, i.e., Fluorescein-5-isothiocyanate (FITC), to perform imaging in the cell. The results highlighted the goodness of the synthesis procedure, as well as the high internalization rate that resulted in an optimal fluorescence intensity. Thus, this work presents a good sustainable/green approach-mediated polymer nanocomposite for various applications in the field of diagnostic imaging.

Keywords: gold nanoparticles; green synthesis; biomedical; fluorescent

Citation: Matteis, V.D.; Rizzello, L.; Cascione, M.; Pellegrino, P.; Singh, J.; Manno, D.; Rinaldi, R. Sustainable Synthesis of FITC Chitosan-Capped Gold Nanoparticles for Biomedical Applications. *Clean Technol.* **2022**, *4*, 942–953. https://doi.org/10.3390/cleantechnol4040058

Academic Editor: Patricia Luis

Received: 8 August 2022
Accepted: 21 September 2022
Published: 30 September 2022

1. Introduction

Chitosan is a polysaccharide material derived from the deacetylation of chitin obtained from exoskeletons of insects and crustaceans [1]. As a consequence of meat extraction from crustaceans, a great amount of shell waste is produced, which represents 40–60% of the total animal weight. As it is necessary to reuse the waste, among different strategies, chitin and chitosan extractions represent a good choice [2].

In addition, a recent study [3,4] regarding the environmental and economic viability of chitosan production in Guayas, Ecuador, suggested that this activity was economically profitable in terms of costs without an environmental impact and with a rate of return of 67.31%.

In addition, chitosan is a biocompatible and low toxic material widely used in biological and medical applications [5]. In addition to its eco-friendly nature, chitosan shows

unique physicochemical properties such as a positive charge [6], different viscosity [7], and high solubility in water due to the conspicuous presence of ammino and hydroxylic groups in its chemical structure [8,9]. Chitosan has also antibacterial and anticancer properties, enhancing internalization through the cross of the negatively charged surfaces such as cell membranes [10]. However, its use as a reducing agent to obtain metallic NPs, such as AuNPs, is not very widespread in the literature, even though the combination of the metal with chitosan is particularly advantageous in the field of nanomedicine [11,12]. In particular, AuNPs are suitable to prevent the agglomeration and precipitation of NPs [13] due to their unique properties regarding the chelation of metal ions, forming van der Waals bonds on the NP surface. In addition, compared with conventional heating, microwave irradiation is a green method, which reduces energy consumption, increasing the reaction uniformity as demonstrated in [14]. In different studies, the AuNPs obtained by CS employed tetrachloroauric acid and microwaves, often using constant power levels [15–17].

However, the size distribution in a specific range was very variable; in particular, for our purpose, i.e., biomedical applications, it was necessary to have a size of about 15 nm. This specific size was less toxic [18] than others even at higher concentrations [19], exhibiting better tissue penetration, great circulation in blood, and optimal clearance, making them powerful tools in drug delivery applications. In addition, the size of 15 nm was suitable for bioimaging, for example, for application in Computed Tomography (CT) [20]

In addition, given the increasing attention to the environment, it is necessary that chemical syntheses became as safe as possible and with low time consumption and equipment in terms of energy [21,22]. In this context, the use of microwaves for inorganic NP synthesis was particularly advantageous because the route is fast and requires low reaction volumes [23]. In addition, the heating in the reaction flask containing the precursors is homogenous, unlike other types of synthetic procedures [24].

For this reason, in this work, AuNPs were synthesized using chitosan as a reducing agent. Au shows several interesting properties; among these, Localized Surface Resonance (LSR) has the most important optical properties [25,26]. Indeed, their inert chemical nature and low toxic behavior make them optimal tools for medical employment [27], in particular, for photothermal therapy treatment [28,29]. The synthesis was carried out in a domestic microwave oven with a reaction time of about 2 min. Therefore, our synthetic approach appears to be eco-friendly and mostly appears to fall within the principles of green chemistry, which are based on the recovery of waste sources (such as crustacean exoskeletons) to create products without the involvement of toxic agents [30–36].

In this way, monodisperse AuNPs with a chitosan shell (AuNPs@CS) were synthesized in the present work with a specific size of 15 nm, perfectly suitable for biomedical applications. These new nanostructures, after being characterized by Transmission Electron Microscopy (TEM), UV–vis, Fourier-transform infrared spectroscopy (FTIR), Dynamic Light Scattering (DLS), and Zeta Potential, were used to be functionalized with a fluorophore, namely, Fluorescein-5-isothiocyanate (FITC). This step allowed us to track their internalization in HeLa cells by confocal microscopy. In the future, the combination between fluorescence and photothermal therapy will be tested by exploiting the properties of Au to increase the anticancer potential of these structures.

2. Materials and Methods

2.1. Synthesis of Gold Nanoparticles by Chitosan Using a Microwave Oven

The synthesis of AuNPs@CS was performed using 1 mL of $HAuCl_4$ (Sigma-Aldrich, Dorset, UK) at concentration of 1 mM and chitosan medium molecular weight (Sigma-Aldrich, Dorset, UK) at concentration of 2% (100 uL). The two solutions were mixed in a glass vial and then transferred to a microwave oven. After 2 min, the solution turned from light yellow to deep red applying 400 W of power. Then, the solution was centrifuged for 30 min at 7000 rpm to collect NPs.

2.2. Functionalization of AuNPs@CS by FITC

The AuNPs@CS were washed several times in water to eliminate any unreacted reaction products. Then, an amount of FITC (Sigma-Aldrich, Dorset, UK) dissolved in ethanol (2 mg/mL^{-1}) was added to AuNPs@CS solution in a concentration range of 500 uM^{-1} mM. The solution was put under stirring overnight in the dark at room temperature to permit the bond between the amino groups of chitosan with isothiocyanate groups. The labeled AuNPs@CS were centrifugated at 13,000 rpm for 20 min and washed several times until no detectable fluorescence was measured in the supernatant. The collected AuNPs@CS-FITC were stored at 4 °C in the dark before use. The synthetic steps were reported in Figure 1.

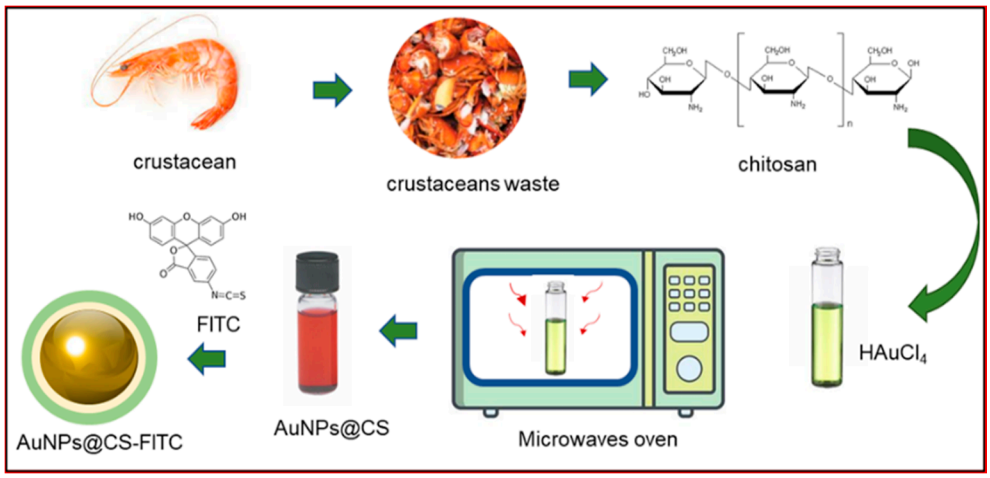

Figure 1. Schematic representation of AuNPs@CS-FITC achievement.

2.3. Characterization of AuNPs@CS-FITC

The morphological characterization of NPs was performed by TEM. The microscope model was a HITACHI 7700 (Tokyo, Japan) operating at 120 Kv. A few NPs dissolved in water were dropped on the carbon-supported 400-mesh copper grid. On TEM images, a statistical analysis was performed by using ImageJ software (National Institutes of Health, USA) on 70 NPs with particle analysis plugin. The DLS and ζ-potential measurements were acquired by a Zetasizer Nano-ZS (ZEN3600, Malvern Instruments Ltd., Malvern, UK), with a HeNe laser (4.0 mW) working at 633 nm detector in aqueous solutions (25 °C, pH 7). The FTIR measurements in the spectral range 400–4000 cm^{-1} were obtained at a resolution of 4 cm^{-1} using a Jasco-670 (Jasco, Tokyo, Japan), whereas UV–vis absorption was recorded by a Shimadzu-2550 (Kyoto, Japna) with 1 cm quartz cuvettes. The emission absorption spectra were measured using an LS-55 spectrophotometer (PerkinElmer, Waltham, MA, USA).

2.4. Cell Culture

Human cervix carcinoma (Hela, Sigma-Aldrich, Dorset, UK) was seeded in high glucose Dulbecco's Modified Eagle Medium (DMEM, Sigma-Aldrich, Dorset, UK) with 50 µM of glutamine, 10% FBS, 100 U/mL penicillin, and 100 mg/mL streptomycin. Cells were maintained at 37 °C in a humidified controlled atmosphere with a 95% of air and a 5% ratio of CO_2.

2.5. Metal Content Measurement by Inductively Coupled Plasma Optical Emission Spectrometry (ICP-OES)

HeLa cells (1×10^5) were seeded in 1 mL of the medium in a multiwell. After 24 h, the medium was removed and replaced with DMEM containing AuNPs@CS-FITC (1 ug/mL, 5 ug/mL, and 10 ug/mL) for 24 h and 48 h. After exposure, the culture medium was removed. Several washes with Phosphate-Buffered Saline (PBS) were performed to eliminate the NPs left in suspension. Cells were separated and counted using an automatic

cell counting chamber as described in [37]. The solution was analyzed to evaluate the ppm of Au using an ICP-OES Perkin Elmer AVIO 500.

2.6. MTT Assay

HeLa cells were seeded in 96-well microplates (5000 cells/well) at final volume of 50 µL and incubated for 24 h. AuNPs@CS-FITC were dispersed in DMEM at three concentrations: 1 ug/mL, 5 ug/mL, and 10 ug/mL in 100 µL for each well for 24 h and 48 h. WST-8 assay (Sigma-Aldrich, Dorset, UK) was performed following the procedure previously described in [38]. Data were expressed as mean ± SD.

2.7. Confocal Microscopy Analysis and Fluorescence Quantification

HeLa cells were seeded (7×10^4 cells/mL) in glass Petri dishes. After 24 h of stabilization, DMEM was displaced and replaced with AuNPs@CS-FITC (10 ug/mL) at 3 h, 12 h, 24 h, and 48 h. After, NPs were removed, and the cells were washed with PBS. Glutaraldehyde (0.25%) was used to fix samples for 10 min followed by a permeabilization step with Triton X-100 (0.1%) for 5 min.

Two different dyes were used for plasma membrane and nuclei labeling, i.e., CellMask™ Deep Red Plasma Membrane Stain (Thermo Fisher Scientific, Waltham, MA, USA), and Dapi (Thermo Fisher Scientific, Waltham, MA, USA). Confocal acquisitions were performed using a Zeiss LSM700 (Carl Zeiss Microscopy GmbH, Munich, Germany) CLSM mounted on an Axio Observer Z1 (Carl Zeiss Microscopy GmbH, Munich, Germany) inverted microscope, using the Alpha Plan-Apochromat (Carl Zeiss Microscopy GmbH, Munich, Germany) 100× oil-immersion objective with 1.46 NA2.10. The fluorescence quantification was performed by ImageJ software. Histograms of red (RC-1) positive pixels were analyzed. The tool "ImageJ/Analyze/Histogram/List" was used, followed by the sum of the counted pixels.

3. Results and Discussion

In this work, the synthesis of AuNPs using chitosan was performed. This nanoplatform was suitable to attach a fluorescent molecule with the aim to develop a safe nanotool for cell imaging.

In this contest, chitosan acting as a green reducing agent controlled the size and the shape-direction, and, at the same time, stabilized the metal NPs making the colloidal solution stable [39]. This is particularly interesting because, in aqueous solution metal, NPs tend to aggregate due to the van der Waals interactions. Chitosan acts as a steric barrier due to the positive charge that permitted the formation of uniform metal NP solutions [40]. In addition, this natural polymer is a valid green alternative reagent to conventional chemical synthesis [41] allowing it to achieve NPs without toxic and hazardous solvents that limit their use in biomedical applications.

Moreover, it has been shown that, from an economic point of view, the use of chitosan is very advantageous. The extraction of chitin from crustacean waste is a simple process and it also allows the elimination of this waste, which represents a disposal problem, especially in sea regions. In this perspective, Riofrio et al. [3] analyzed the environmental impact and the life cycle assessment of chitosan production in Guayas, Ecuador, and concluded that it is economically low coat and safe.

In our work, chitosan and a domestic microwave oven were used to obtain stable nanostructures using a frequency of 2.45 GHz [42]. This frequency permits the oscillation of polar molecules, such as water, to be generated, producing uniform heating [43]. The use of microwaves is particularly suitable as an eco-friendly method for metal NPs because they combine the use of reduced reaction volumes with low energy consumption [44]. In addition, the procedure is easy with a high reproducibility rate. First, we proceed to optimize the chitosan concentration with the time of reaction (2 min) and the power of microwaves (400 W) kept constant to obtain good AuNPs@CS. Using 0.5% and 1% chitosan concentrations, the solutions changed color from light yellow to light red suggesting the

start of the reduction process from Au ions into Au atoms. Using a 2% CS concentration, the solution became dark red suggesting the formation of NP chitosan-capped AuNPs (Figure 2).

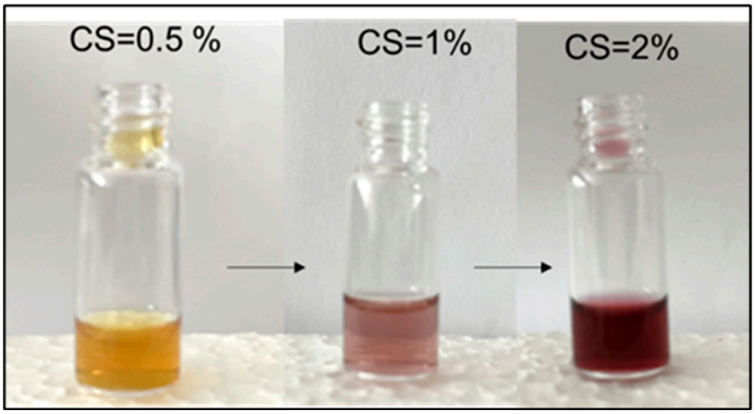

Figure 2. Color change in $HAuCl_4$ solution (1 mM) modifying CS concentration.

The TEM acquisitions (Figure 3a–c) showed the morphology of AuNPs@CS-FITC that were perfectly round and monodispersed. In addition, no organic residues were visible. On the other hand, the presence of a clear visible low-contrast organic shell on the AuNPs surface was noted, demonstrating the efficacy of chitosan to work also as a capping agent. The mean size distribution, measured by ImageJ analysis, was around (14.5 ± 0.2) nm (Figure 3d). The statistical analysis was conducted by selecting 70 nano-objects for each NP to perform a Gaussian fitting.

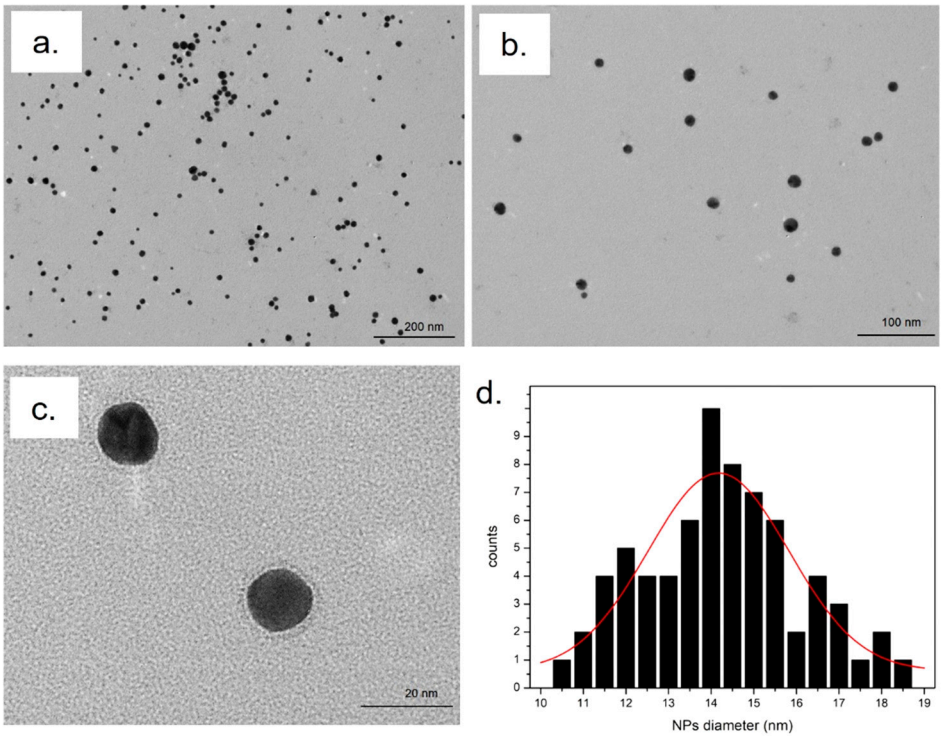

Figure 3. TEM images of AuNPs@CS-FITC obtained by microwave eco-friendly synthesis at different magnifications: 200 nm (**a**), 100 nm (**b**), and 20 nm (**c**). Statistical analysis with Gaussian fit (red line) for AuNPs@CS-FITC (**d**).

DLS measurements on AuNPs@CS-FITC (in water) confirmed the TEM data and showed NPs with a hydrodynamic radius of (15 ± 2). The surface charge was positive in

water (+32 ± 3) mV due to the presence of amino groups associated with the chitosan shell (Table 1).

Table 1. Characterization of AuNPs@CS in water and DMEM by DLS and ζ-potential (mV) measurements.

	Size (nm) in Water	**ζ-Potential (mV ±) in Water**
AuNPs@CS	15 ± 2	+32 ± 2
	Size (nm) in DMEM	**ζ-Potential (mV ±) in DMEM**
AuNPs@CS	23 ± 4	−30 ± 3

The obtained size (c.a 15 nm) is particularly interesting for the goal sought in this work, since it is the optimal size to use in biomedical applications showing low toxicity and high penetration rate; these two properties are very important for imaging applications in which a high rate of internalization is required [18].

DLS and ζ potential characterizations were also performed in the cell culture growth media, namely, DMEM, as these nanostructures were developed for imaging in cells. An increase in the NP size was shown, which was probably due to the protein corona influencing the ζ potential value, which became negative.

Then, the optical characterization by UV–vis measurements indicating the formation of AuNPs at concentrations of 1% and 2% chitosan was performed. Conversely, the lower concentration, namely, 0.5% chitosan, did not induce noticeable AuNP formation. The plasmonic peak was measured at about 550 nm and 560 nm using 1% and 2% chitosan concentrations, respectively (Figure 4a). Therefore, the prominent peak was observed using the highest concentration, indicating the optimum condition to obtain this kind of material at the same time conditions and power of the microwaves.

The FTIR analysis of AuNPs@CS was performed to recognize the interactions between the Au surface and the chitosan groups (Figure 4b). The spectrum that was related to AuNPs@CS looked similar to that of the correspondent pure chitosan graph. The pure chitosan exhibited specific vibrations in the range of 3357 and 3270 cm^{-1} related to the stretching vibrations of the O-H or N-H groups. The peak observed at c.a. 2850 cm^{-1} corresponded to the vibration of the C-H groups, whereas the N-H bonds (amide II) (NH_2) were observed at 1579 cm^{-1}. The intense peak at 1360 cm^{-1} could be associated with the C-C stretching of the glucosamine group of chitosan, whereas the C-O vibration was shown at 1015 cm^{-1}.

The characteristic peaks in the AuNPs@CS graph were in the range of 3360–3260 cm^{-1} and in the range of 2992–2900 cm^{-1}. The other peaks were the same as those found in the spectra of pure chitosan, demonstrating the functionalization of the Au surface by chitosan [45,46].

The chemical structure of chitosan, characterized by primary amino and secondary hydroxyl groups, lends itself very well to various types of chemical functionalization to improve specific properties. Among different kinds of fluorescent dyes, FITC is a stable, biocompatible, and polar molecule having a high fluorescence emission. The chemical conjugation between the chitosan shell and FITC was through the bond between the amine groups (-NH_2) and isothiocyanate group R-N=C=S, which allowed the AuNPs@CS-FITC by thiourea linkage to be obtained. Then, the fluorescence properties of AuNPs@CS-FITC were carefully investigated using the excitation wavelength of 488 nm. In Figure 5, it was possible to note that the peak associated with NPs was slightly red shifted (522 nm) with respect to pure FITC (518 nm). This movement can be explained by the amino groups of chitosan or, as a second hypothesis, by the connection between dye and metal NPs as reported in a previous study [47].

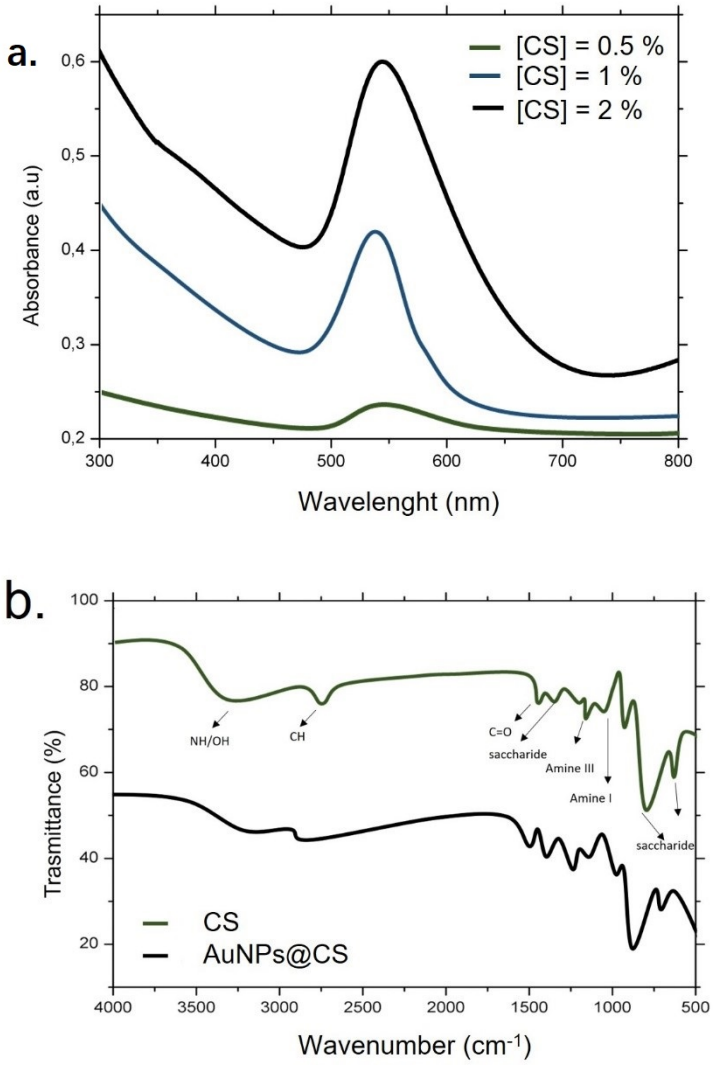

Figure 4. (**a**) UV–vis spectra of AuNPs@CS using different chitosan concentration (0.5%, 1%, and 2%) (**b**). FTIR spectra of pure medium chitosan and AuNPs@CS.

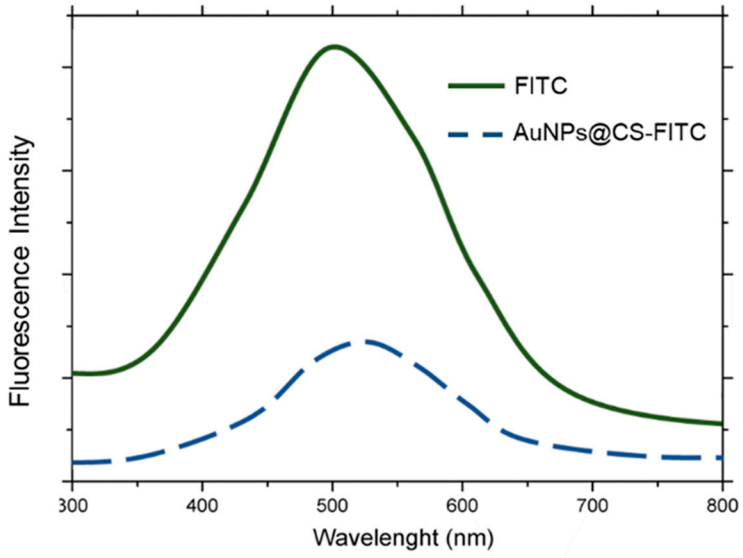

Figure 5. Emission spectra (λex = 488 nm) of FITC and AuNPs@CS-FITC.

After physical and chemical characterizations, the ability of AuNPs@CS-FITC to work as an imaging agent was verified by choosing the epithelioid cervix carcinoma human cell line (HeLa) as the model system. Firstly, we assessed the cell viability, which showed no significant toxicity using the three concentrations of NPs chosen in this study (1 ug/mL, 5 ug/mL, and 10 ug/mL) and the two time points (24 h and 48 h) (Figure 6a).

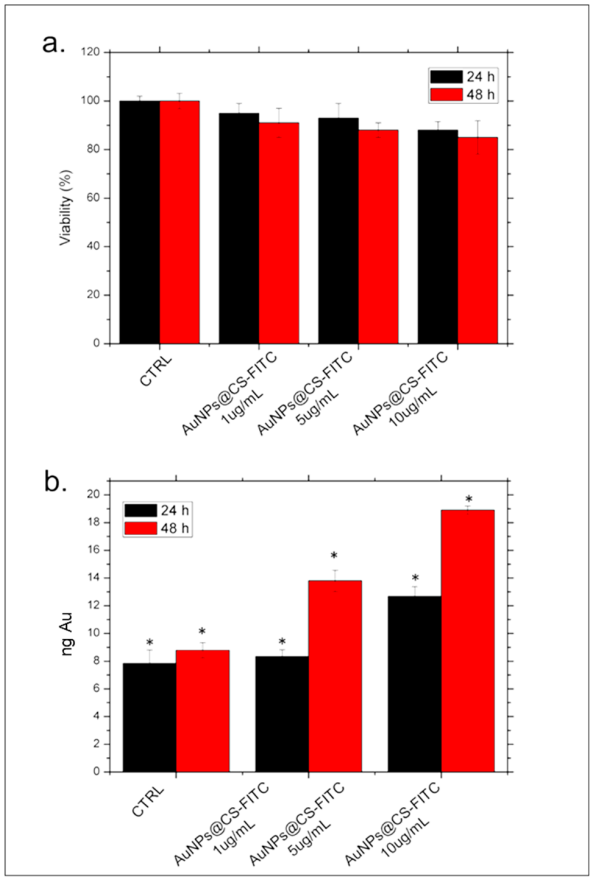

Figure 6. (**a**). Viability assay performed on HeLa cell lines exposed to 1 ug/mL, 5 ug/mL, and 10 ug/mL of AuNPs@CS-FITC after 24 h and 48 h. The viability of cells exposed to NPs was normalized to control cells (untreated). As a positive control (P), 5% of DMSO was used (data not shown). Data were reported as the mean ± SD from three independent experiments. (**b**). Accumulation in HeLa cell lines exposed to 1 ug/mL, 5 ug/mL, and 10 ug/mL of AuNPs@CS-FITC after 24 h and 48 h. The cells were then harvested, the live cells were counted, and the Au content was measured in 360.000 cells (ng Au). The control was represented by untreated cells (values = 0, data not shown). Data were the mean values of 3 experiments ± SD and they were statistically significant for $p < 0.05$ (*).

Indeed, the reduction in live cells was very low, and it was never below 83%. To connect the data regarding cell death with the NPs uptake, ICP measurements on the HeLa cells after the incubation with the three concentrations of AuNPs@CS-FITC (1 ug/mL, 5 ug/mL, and 10 ug/mL) were taken. As observed in Figure 6b, the internalization was dose and time dependent. After 48 h, at the highest concentration tested, the amount of Au was 18.4 ng, indicating that these NPs can be used for imaging purposes due to the high uptake rate, as expected.

After the quantification of the internalization properties in terms of the Au amount, the uptake was investigated through fluorescent quantification of the time. The higher concentration of AuNPs@CS-FITC (10 ug/mL) was chosen due to the higher efficacy in the endocytosis event. Hela cells were observed at four different time points (3 h, 6 h, 12 h, 24 h, and 48 h). At the end of each time, cells were fixed and labeled to visualize the actin

and nucleus structure (Figure 7). As can be seen, the fluorescence intensity became higher when the time increased with respect to the control cells (Figure 7a,b). Starting from 3 h (Figure 7c,d), an increasing fluorescence intensity at 12 h (Figure 7e,f) was observed. After 48 h, it was possible to note the maximum fluorescence intensity showing a prominent localization in the cell cytosol (Figure 7i,j). The intensity of fluorescence was calculated on confocal images using ImageJ software (Figure 7k), confirming the data obtained by confocal observations.

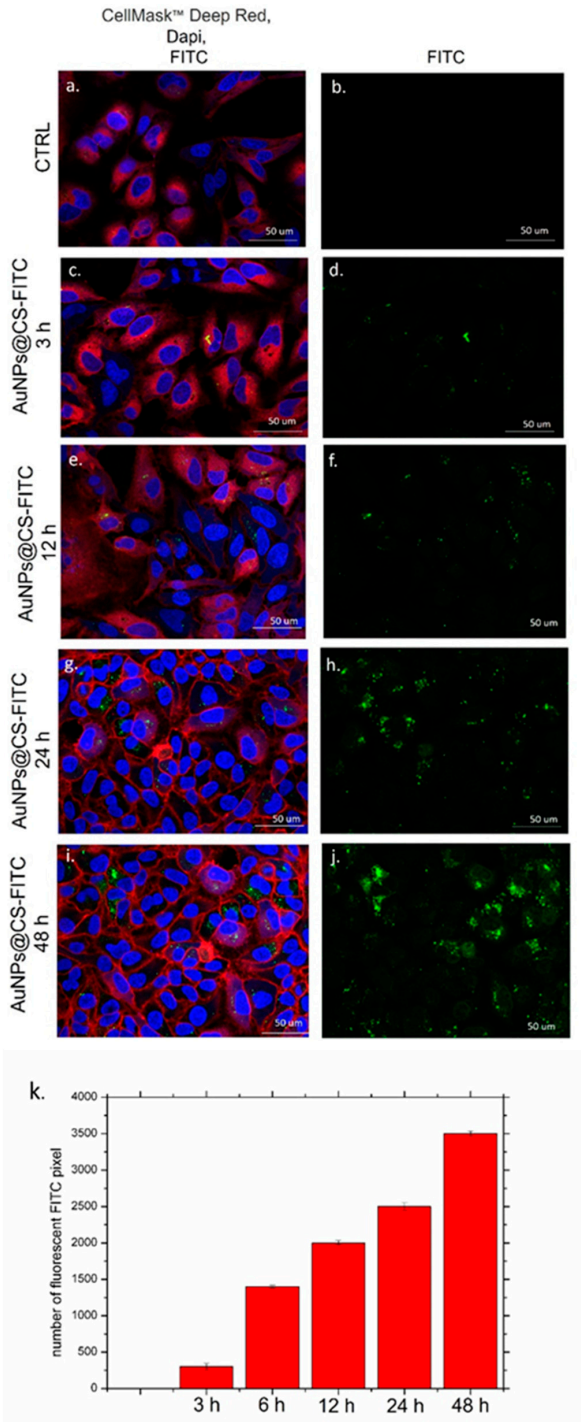

Figure 7. Confocal acquisitions of HeLa cells labeled by cellMask and Dapi to visualize actin (red) and nuclei (blue) (**a**,**c**,**e**,**g**,**i**) and relative green fluorescent (**b**,**d**,**f**,**h**,**j**) related to the internalization of AuNPs@CS-FITC in the time (0, 3, 6, 12, 24, 48 h). Fluorescence analysis conducted on confocal acquisitions using ImageJ software (**k**).

All the experimental results corroborated the hypothesis that AuNPs@CS-FITC can be used as safe agents for imaging in vitro. In particular, the smaller size of NPs can be useful to visualize their accumulation in specific organelles, allowing high-resolution images to be carried out. The same protocol can be applied to visualize also other kinds of cells, both tumoral and healthy.

4. Conclusions

In conclusion, AuNPs were successfully synthesized via a green approach using chitosan, a natural polymer with unique properties. This approach is extremely convenient in terms of low time and energy consumption, as well as the absence of toxic substances in the synthetic route.

TEM results showed the morphology of NPs, which was perfectly round; AuNPs were monodispersed with a diameter of 14.5 ± 0.2 nm, particularly suitable for medicine application since this size permits a high uptake rate and low toxicity to be obtained. FTIR study elucidated the strong capping of AuNPs by chitosan, which confirmed the formation of the AuNPs@CS complex. Furthermore, the new nanoplatform can be used as a tool to visualize cellular compartments functionalizing the chitosan shell with a fluorescent molecule, namely, FITC, following their internalization in cell models after different time points. Further experiments will be carried out to combine imaging with thermal therapy since AuNPs play an important role due to their high thermal conductivity. This is possible thanks to the low toxicity of the NPs, also helped by the presence of chitosan as a capping agent.

Author Contributions: Conceptualization, V.D.M., methodology, L.R., M.C., D.M. and J.S.; validation V.D.M. and L.R.; formal analysis V.D.M.; data curation, V.D.M., L.R. and J.S.; writing—original draft preparation, V.D.M.; editing, V.D.M., L.R., M.C., P.P., D.M., J.S. and R.R.; supervision, V.D.M.; project administration, V.D.M. and R.R. All authors have read and agreed to the published version of the manuscript.

Funding: This research received no external funding.

Institutional Review Board Statement: Not applicable.

Informed Consent Statement: Not applicable.

Data Availability Statement: The data presented in this study are available in this article.

Acknowledgments: V.D.M. kindly acknowledges Programma Operativo Nazionale (PON) Ricerca e Innovazione 2014-20202014-azione IV.6 "Contratti su tematiche green"-DM 1062/2021 for sponsoring her salary and work. L.R. sincerely acknowledges the ERC-2.019-STG (grant number 850936) and the Fondazione Cariplo (grant number 2019-4278) for sponsoring his salary and work. M.C. kindly acknowledge the Programma Operativo Nazionale (PON) Ricerca e Innovazione 2014-2020 Asse I Capitale Umano, Azione I.2, Avviso 'A.I.M: Attraction and International Mobility for sponsor their salary and work.

Conflicts of Interest: The authors declare no conflict of interest.

References

1. Adhikari, H.S.; Yadav, P.N. Anticancer Activity of Chitosan, Chitosan Derivatives, and Their Mechanism of Action. *Int. J. Biomater.* **2018**, *2018*, 1–29. [CrossRef] [PubMed]
2. Fatnah, N.; Azizah, D.; Cahyani, M.D. Synthesis of Chitosan from Crab's Shell Waste (Portunus pelagicus) in Mertasinga-Cirebon. In *International Conference on Progressive Education (ICOPE 2019)*; Atlantis Press: Amsterdam, The Netherlands, 2020. Available online: https://www.atlantis-press.com/proceedings/icope-19/125937567 (accessed on 1 August 2022).
3. Riofrio, A.; Alcivar, T.; Baykara, H. Environmental and Economic Viability of Chitosan Production in Guayas-Ecuador: A Robust Investment and Life Cycle Analysis. *ACS Omega* **2021**, *6*, 23038–23051. [CrossRef] [PubMed]
4. Gómez-Ríos, D.; Barrera-Zapata, R.; Ríos-Estepa, R. Comparison of process technologies for chitosan production from shrimp shell waste: A techno-economic approach using Aspen Plus ®. *Food Bioprod. Process.* **2017**, *103*, 49–57. [CrossRef]
5. Rodrigues, S.; Dionísio, M.; López, C.R.; Grenha, A. Biocompatibility of Chitosan Carriers with Application in Drug Delivery. *J. Funct. Biomater.* **2012**, *3*, 615–641. [CrossRef]

6. Mohammed, M.A.; Syeda, J.T.M.; Wasan, K.M.; Wasan, E.K. An Overview of Chitosan Nanoparticles and Its Application in Non-Parenteral Drug Delivery. *Pharmaceutics* **2017**, *9*, 53. [CrossRef]
7. Costa, C.N.; Teixeira, V.G.; Delpech, M.C.; Souza, J.V.S.; Costa, M.A. Viscometric study of chitosan solutions in acetic acid/sodium acetate and acetic acid/sodium chloride. *Carbohydr. Polym.* **2015**, *133*, 245–250. [CrossRef]
8. Wan, M.-C.; Qin, W.; Lei, C.; Li, Q.-H.; Meng, M.; Fang, M.; Song, W.; Chen, J.-H.; Tay, F.; Niu, L.-N. Biomaterials from the sea: Future building blocks for biomedical applications. *Bioact. Mater.* **2021**, *6*, 4255–4285. [CrossRef]
9. Bai, L.; Liu, L.; Esquivel, M.; Tardy, B.L.; Huan, S.; Niu, X.; Liu, S.; Yang, G.; Fan, Y.; Rojas, O.J. Nanochitin: Chemistry, Structure, Assembly, and Applications. *Chem. Rev.* **2022**, *122*, 11604–11674. [CrossRef]
10. Sharifi-Rad, J.; Quispe, C.; Butnariu, M.; Rotariu, L.S.; Sytar, O.; Sestito, S.; Rapposelli, S.; Akram, M.; Iqbal, M.; Krishna, A.; et al. Composite materials based on chitosan/gold nanoparticles: From synthesis to biomedical applications. *Int. J. Biol. Macromol.* **2020**, *161*, 977–998. [CrossRef]
11. Huang, H.; Yang, X. Martins, Synthesis of Chitosan-Stabilized Gold Nanoparticles in the Absence/Presence of Tripolyphosphate. *Biomacromolecules* **2004**, *5*, 2340–2346. [CrossRef]
12. Phan, T.; Phan, D.; Cao, X.; Huynh, T.-C.; Oh, J. Roles of Chitosan in Green Synthesis of Metal Nanoparticles for Biomedical Applications. *Nanomaterials* **2021**, *11*, 273. [CrossRef]
13. Bin Ahmad, M.; Lim, J.J.; Shameli, K.; Ibrahim, N.A.; Tay, M.Y. Synthesis of Silver Nanoparticles in Chitosan, Gelatin and Chitosan/Gelatin Bionanocomposites by a Chemical Reducing Agent and Their Characterization. *Molecules* **2011**, *16*, 7237–7248. [CrossRef]
14. Madhavan, V.; Gangadharan, P.K.; Ajayan, A.; Chandran, S.; Raveendran, P. Microwave-assisted solid-state synthesis of Au nanoparticles, size-selective speciation, and their self-assembly into 2D-superlattice. *Nano-Struct. Nano-Objects* **2019**, *17*, 218–222. [CrossRef]
15. Thanayutsiri, T.; Patrojanasophon, P.; Opanasopit, P.; Ngawhirunpat, T.; Plianwong, S.; Rojanarata, T. Rapid synthesis of chitosan-capped gold nanoparticles for analytical application and facile recovery of gold from laboratory waste. *Carbohydr. Polym.* **2020**, *250*, 116983. [CrossRef]
16. Hashem, A.H.; Shehabeldine, A.M.; Ali, O.M.; Salem, S.S. Synthesis of Chitosan-Based Gold Nanoparticles: Antimicrobial and Wound-Healing Activities. *Polymers* **2022**, *14*, 2293. [CrossRef]
17. Fan, C.; Li, W.; Zhao, S.; Chen, J.; Li, X. Efficient one pot synthesis of chitosan-induced gold nanoparticles by microwave irradiation. *Mater. Lett.* **2008**, *62*, 3518–3520. [CrossRef]
18. Anik, M.I.; Mahmud, N.; Al Masud, A.; Hasan, M. Gold nanoparticles (GNPs) in biomedical and clinical applications: A review. *Nano Sel.* **2021**, *3*, 792–828. [CrossRef]
19. Bansal, S.A.; Kumar, V.; Karimi, J.; Singh, A.P.; Kumar, S. Role of gold nanoparticles in advanced biomedical applications. *Nanoscale Adv.* **2020**, *2*, 3764–3787. [CrossRef]
20. Dong, Y.C.; Hajfathalian, M.; Maidment, P.S.N.; Hsu, J.C.; Naha, P.C.; Si-Mohamed, S.; Breuilly, M.; Kim, J.; Chhour, P.; Douek, P.; et al. Effect of Gold Nanoparticle Size on Their Properties as Contrast Agents for Computed Tomography. *Sci. Rep.* **2019**, *9*, 1–13. [CrossRef]
21. De Matteis, V.; Rizzello, L.; Cascione, M.; Liatsi-Douvitsa, E.; Apriceno, A.; Rinaldi, R. Green Plasmonic Nanoparticles and Bio-Inspired Stimuli-Responsive Vesicles in Cancer Therapy Application. *Nanomaterials* **2020**, *10*, 1083. [CrossRef]
22. Gómez-López, P.; Puente-Santiago, A.; Castro-Beltrán, A.; Nascimento, L.A.S.D.; Balu, A.M.; Luque, R.; Alvarado-Beltrán, C.G. Nanomaterials and catalysis for green chemistry. *Curr. Opin. Green Sustain. Chem.* **2020**, *24*, 48–55. [CrossRef]
23. Wu, Z.; Borretto, E.; Medlock, J.; Bonrath, W.; Cravotto, G. Effects of Ultrasound and Microwaves on Selective Reduction: Catalyst Preparation and Reactions. *ChemCatChem* **2014**, *6*, 2762–2783. [CrossRef]
24. Gawande, M.B.; Shelke, S.N.; Zboril, R.; Varma, R.S. Microwave-Assisted Chemistry: Synthetic Applications for Rapid Assembly of Nanomaterials and Organics. *Acc. Chem. Res.* **2014**, *47*, 1338–1348. [CrossRef]
25. Dykman, L.A.; Khlebtsov, N.G. Gold Nanoparticles in Biology and Medicine: Recent Advances and Prospects. *Acta Nat.* **2011**, *3*, 34–55. [CrossRef]
26. De Matteis, V.; Rizzello, L. Noble Metals and Soft Bio-Inspired Nanoparticles in Retinal Diseases Treatment: A Perspective. *Cells* **2020**, *9*, 679. [CrossRef]
27. De Matteis, V.; Cannavale, A.; Blasi, L.; Quarta, A.; Gigli, G. Chromogenic device for cystic fibrosis precocious diagnosis: A "point of care" tool for sweat test. *Sens. Actuators B Chem.* **2016**, *225*, 474–480. [CrossRef]
28. De Matteis, V.; Cascione, M.; Rizzello, L.; Manno, D.; Di Guglielmo, C.; Rinaldi, R. Synergistic Effect Induced by Gold Nanoparticles with Polyphenols Shell during Thermal Therapy: Macrophage Inflammatory Response and Cancer Cell Death Assessment. *Cancers* **2021**, *13*, 3610. [CrossRef]
29. Norouzi, H.; Khoshgard, K.; Akbarzadeh, F. In vitro outlook of gold nanoparticles in photo-thermal therapy: A literature review. *Lasers Med Sci.* **2018**, *33*, 917–926. [CrossRef]
30. Singh, J.; Dutta, T.; Kim, K.-H.; Rawat, M.; Samddar, P.; Kumar, P. 'Green' synthesis of metals and their oxide nanoparticles: Applications for environmental remediation. *J. Nanobiotechnol.* **2018**, *16*, 84. [CrossRef]
31. Parmar, S.; Kaur, H.; Singh, J.; Matharu, A.S.; Ramakrishna, S.; Bechelany, M. Recent Advances in Green Synthesis of Ag NPs for Extenuating Antimicrobial Resistance. *Nanomaterials* **2022**, *12*, 1115. [CrossRef]

32. Verma, V.; Al-Dossari, M.; Singh, J.; Rawat, M.; Kordy, M.G.M.; Shaban, M. A Review on Green Synthesis of TiO_2 NPs: Photocatalysis and Antimicrobial Applications. *Polymers* **2022**, *14*, 1444. [CrossRef] [PubMed]
33. Rani, P.; Ahmed, B.; Singh, J.; Kaur, J.; Rawat, M.; Kaur, N.; Matharu, A.S.; AlKahtani, M.; Alhomaidi, E.A.; Lee, J. Silver nanostructures prepared via novel green approach as an effective platform for biological and environmental applications. *Saudi J. Biol. Sci.* **2022**, *29*. [CrossRef] [PubMed]
34. Singh, J.; Kaur, H.; Rawat, M. A novel green approach for the synthesis of tungsten oxide nanorods and its efficient potential towards photocatalytic degradation of reactive green 19 dye. *J. Mater. Sci. Mater. Electron.* **2018**, *29*, 13715–13722. [CrossRef]
35. Kaur, K.; Ahmed, B.; Singh, J.; Rawat, M.; Kaur, G.; AlKahtani, M.; Alhomaidi, E.A.; Lee, J. Bryonia laciniosa Linn mediated green synthesized Au NPs for catalytic and antimicrobial applications. *J. King Saud Univ. Sci.* **2022**, *34*, 102022. [CrossRef]
36. Singh, J.; Kumar, V.; Jolly, S.S.; Kim, K.-H.; Rawat, M.; Kukkar, D.; Tsang, Y.F. Biogenic synthesis of silver nanoparticles and its photocatalytic applications for removal of organic pollutants in water. *J. Ind. Eng. Chem.* **2019**, *80*, 247–257. [CrossRef]
37. De Matteis, V.; Rizzello, L.; Di Bello, M.P.; Rinaldi, R. One-step synthesis, toxicity assessment and degradation in tumoral pH environment of SiO2@Ag core/shell nanoparticles. *J. Nanoparticle Res.* **2017**, *19*. [CrossRef]
38. De Matteis, V.; Rizzello, L.; Ingrosso, C.; Liatsi-Douvitsa, E.; De Giorgi, M.L.; De Matteis, G.; Rinaldi, R. Cultivar-Dependent Anticancer and Antibacterial Properties of Silver Nanoparticles Synthesized Using Leaves of Different Olea Europaea Trees. *Nanomaterials* **2019**, *9*, 1544. [CrossRef]
39. Collado-González, M.; Montalbán, M.G.; Peña-García, J.; Pérez-Sánchez, H.; Víllora, G.; Díaz Baños, F.G. Chitosan as stabilizing agent for negatively charged nanoparticles. *Carbohydr. Polym.* **2017**, *161*, 63–70. [CrossRef]
40. Franconetti, A.; Carnerero, J.M.; Prado-Gotor, R.; Cabrera-Escribano, F.; Jaime, C. Chitosan as a capping agent: Insights on the stabilization of gold nanoparticles. *Carbohydr. Polym.* **2018**, *207*, 806–814. [CrossRef]
41. Frank, L.A.; Onzi, G.R.; Morawski, A.S.; Pohlmann, A.R.; Guterres, S.S.; Contri, R.V. Chitosan as a coating material for nanoparticles intended for biomedical applications. *React. Funct. Polym.* **2019**, *147*, 104459. [CrossRef]
42. Bilecka, I.; Niederberger, M. Microwave chemistry for inorganic nanomaterials synthesis. *Nanoscale* **2010**, *2*, 1358–1374. [CrossRef]
43. Zhu, Y.J.; Chen, F. Microwave-Assisted Preparation of Inorganic Nanostructures in Liquid Phase. *Chem. Rev.* **2014**, *114*, 6462–6555. [CrossRef]
44. Ahmed, S.F.; Mofijur, M.; Rafa, N.; Chowdhury, A.T.; Chowdhury, S.; Nahrin, M.; Islam, A.S.; Ong, H.C. Green approaches in synthesising nanomaterials for environmental nanobioremediation: Technological advancements, applications, benefits and challenges. *Environ. Res.* **2021**, *204*, 111967. [CrossRef]
45. Mohan, C.O.; Gunasekaran, S.; Ravishankar, C.N. Chitosan-capped gold nanoparticles for indicating temperature abuse in frozen stored products. *NPJ Sci. Food* **2019**, *3*, 1–6. [CrossRef]
46. Inbaraj, B.S.; Chen, B.-Y.; Liao, C.-W.; Chen, B.-H. Green synthesis, characterization and evaluation of catalytic and antibacterial activities of chitosan, glycol chitosan and poly(γ-glutamic acid) capped gold nanoparticles. *Int. J. Biol. Macromol.* **2020**, *161*, 1484–1495. [CrossRef]
47. Ge, Y.; Zhang, Y.; He, S.; Nie, F.; Teng, G.; Gu, N. Fluorescence Modified Chitosan-Coated Magnetic Nanoparticles for High-Efficient Cellular Imaging. *Nanoscale Res. Lett.* **2009**, *4*, 287–295. [CrossRef]